

Raman Scattering in FeBO₃ at High Pressures: Phonon Coupled to Spin-Pair Fluctuations and Magnetodeformation Potentials

M. J. Massey^(a) and R. Merlin

The Harrison M. Randall Laboratory of Physics, The University of Michigan, Ann Arbor, Michigan 48109-1120

S. M. Girvin

Department of Physics, Indiana University, Bloomington, Indiana 47405

(Received 20 July 1992)

The first direct measurement of the modulation of the magnetic superexchange parameter J by optical phonons is reported. High-pressure Raman scattering studies of the model compound FeBO₃ reveal an unexpectedly large interaction between a (BO₃)³⁻ internal mode and spin-pair excitations. By pressure tuning J , resonant decay of the phonon into the two-magnon continuum and associated mixing were observed yielding a phonon-magnon-pair coupling constant $g \approx (0.15-0.20)J$.

PACS numbers: 75.50.Ee, 75.30.Et, 75.80.+q, 78.30.Hv

We report the first direct observation of the modulation of the superexchange parameter J in a magnetic material arising from optical phonon distortions. The physics of this modulation mechanism is of interest because of its potential relevance to the spin fluctuation spectrum in a wide variety of magnetic materials possibly including high-temperature superconductors and their insulating parent compounds where a number of mysteries remain unsolved [1]. Here, we present a high-pressure Raman scattering study of the model antiferromagnet FeBO₃ [2,3] in which we found relatively large changes of J due to ion displacements at optical frequencies.

In magnetic insulators whose low-lying electronic excitations are described by the Heisenberg Hamiltonian [4], the electron-phonon coupling V manifests itself through the modulation of the exchange interaction by the vibrations. To lowest order in Q ,

$$V = \sum_{m>p} \left(\frac{\partial J_{mp}}{\partial Q} \bigg|_{Q=0} \right) Q \mathbf{S}_m \cdot \mathbf{S}_p, \quad (1)$$

where \mathbf{S}_l is the spin localized at the l th lattice site and Q is a phonon coordinate operator. The exchange integral J_{mp} depends on the relative positions of sites m and p and, therefore, on Q . By analogy with usage for the conventional semiconductor and metal counterparts [5], the coefficients $\partial J_{mp}/\partial Q$ will be referred to as magnetic deformation potentials [6].

Much of the understanding of V comes from early magnetostriction (or exchange-) striction work bearing primarily on the interaction with acoustic phonons [7]. These modes are also relevant to a possible magnetic isotope effect [8] and, more generally, to measurements of the pressure dependence of magnetic parameters [9]. In this work, the focus is on optical phonons. Coupling between spin pairs and optical modes has been considered theoretically (including a proposal for phonon-mediated Raman scattering by magnon pairs) [10] but, to the best of our knowledge, there have so far been no experimental studies [11]. We chose the model compound FeBO₃ [2,3]

because, at ambient pressure, its Raman spectrum exhibits an internal (BO₃)³⁻ vibration which has the same symmetry (E_g) as, and occurs above the cutoff energy for, $2M$ scattering [12]. By applying high pressures, we were able to tune the $2M$ peak to resonate with the phonon while monitoring the behavior of both excitations using Raman scattering. The Raman spectra exhibit a Fano-like resonance line shape due to mixing of the phonon and the $2M$ continuum from where the magnetic deformation potential can be readily determined.

FeBO₃ crystallizes in the calcite lattice with two formula units per cell (Fig. 1). Its structure consists of

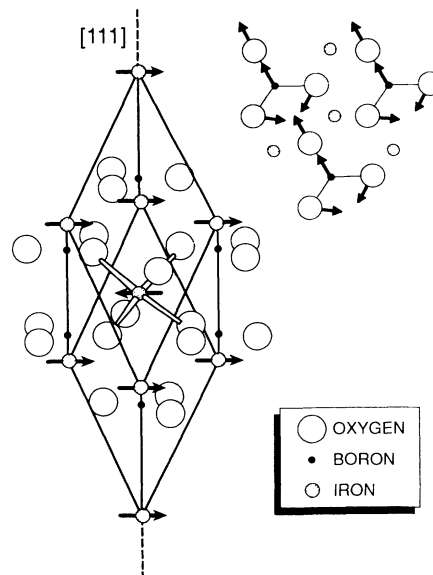


FIG. 1. Crystal structure of FeBO₃. The antiferromagnetic spin configuration is denoted by arrows attached to the cations. Inset: Three-layer projection on a (111) plane. The central Fe³⁺ ion and three (of a total of six) nn cations and anions are indicated. Thinner arrows represent schematically one of the states of the doubly degenerate internal (BO₃)³⁻ mode.

close-packed alternating (111) layers of Fe^{3+} cations and $(\text{BO}_3)^{3-}$ anions in an fcc-like stacking; the point group is D_{3d} [2,3]. The magnetic ions occupy octahedral sites and their ground state is an orbital singlet (${}^6A_{1g}$). Below the Néel temperature $T_N = 348$ K, FeBO_3 orders magnetically with the Fe^{3+} spins ($S = \frac{5}{2}$) lying perpendicular to [111] due to weak anisotropy. Except for a slight canting of the two sublattices, leading to a weak ferromagnetic moment along $[1\bar{1}0]$, the alignment is antiferromagnetic [2,3]. Exchange is dominated by nearest-neighbor (nn) intersublattice interactions with $J = 9.6 \text{ cm}^{-1}$ at ambient pressure [3] (here, we write the Heisenberg Hamiltonian as $H = \sum_{m>p} J_{mp} \mathbf{S}_m \cdot \mathbf{S}_p$ to avoid double counting; note that $J > 0$ for antiferromagnetic coupling). In the following, contributions due to other exchange and anisotropy constants (which are at least an order of magnitude smaller [3]) will be ignored.

In conventional Raman scattering by phonons and spin-pair fluctuations, the D_{3d} representations that matter are A_{1g} and E_g [13]. Within the standard model applying to antiferromagnets, the $2M$ transition operator consists of bilinear combinations involving pairs of spins on opposite sublattices [14]. For the usually dominant nn contribution, such terms can be shown to transform like $A_{1g} + E_g + A_{1u} + E_u$ (six nn pairs). Symmetries A_{1u} and E_u are Raman forbidden. Given that the A_{1g} term is proportional to the Hamiltonian and, thus, that it cannot induce transitions, it follows that pair fluctuations probed by light scattering are of E_g symmetry. This conclusion, based on the neglect of all but nn terms, is supported by experiments [15]. Locally, the E_g spin-pair components can be taken as

$$\lambda_j^\pm = \sum_n e^{\pm(2\pi ni/3)} \mathbf{S}_{\uparrow, r_j} \cdot [\mathbf{S}_{\downarrow, r_j + t_n} + \mathbf{S}_{\downarrow, r_j - t_n}] \quad (2)$$

with vertical arrows denoting the two sublattices. $\mathbf{S}_{\uparrow, r_j}$ is the spin of the central magnetic ion at r_j , while $\mathbf{S}_{\downarrow, r_j \pm t_n}$ and $\pm t_n$ are the spins and the relative positions of its neighbors.

The relevant (doubly degenerate) E_g phonon of the planar $(\text{BO}_3)^{3-}$ group is depicted in the inset of Fig. 1 [16]. The most general linear coupling between $2M$ excitations and the internal mode is given by

$$V = \sum_j [D\lambda_j^+ Q^- + D^* \lambda_j^- Q^+], \quad (3)$$

where D is a constant and $Q^\pm = \pm(i/\sqrt{2})[Q_\alpha + e^{\mp(2\pi i/3)} Q_\beta]$ are orthogonal components transforming like E_g . Q_α and Q_β are displacement operators associated with the motion shown in Fig. 1 and the $(2\pi/3)$ -rotated pattern, respectively.

For a given excitation of symmetry E_g , the Raman cross section is determined by two independent parameters associated with different geometries [13]. If the electric vectors of the incident and scattered photons, \mathbf{E} and $\bar{\mathbf{E}}$, are both orthogonal to the trigonal z axis, the combined scattering Hamiltonian reads

$$H_R = \sum_j r_{2M}^{(x,y)} [\lambda_j^+ W^- + \lambda_j^- W^+] + r_{\bar{p}}^{(x,y)} [Q^+ W^- + Q^- W^+], \quad (4)$$

with $W^\pm = (E_x \bar{E}_x - E_y \bar{E}_y) \pm i(E_x \bar{E}_y + E_y \bar{E}_x)$; $r_{2M}^{(x,y)}$ and $r_{\bar{p}}^{(x,y)}$ are Raman amplitudes for $2M$ and phonon in-plane scattering. The case where either \mathbf{E} or $\bar{\mathbf{E}}$ are parallel to [111] has $W^\pm = (E_x \bar{E}_z - E_z \bar{E}_x) \pm i(E_y \bar{E}_z + E_z \bar{E}_y)$ and two additional amplitudes (say, $r_{2M}^{(z)}$ and $r_{\bar{p}}^{(z)}$). The Raman intensity is $I(\omega) \propto -\text{Im}[G(\omega)]$ where the Green function $G(\omega)$ is the Fourier transform of the correlation function $\langle H_R(t) H_R(0) \rangle$; $H_R(t)$ is H_R [Eq. (4)] in the Heisenberg picture [14]. As it will become evident later, our results focus on hybrid terms involving correlations between the phonon and magnon pairs. We notice that, away from crossing, the spin-pair line shape in FeBO_3 agrees extremely well with the standard theory relying on a mean-field treatment of magnon-magnon interactions [12]. This approach leads to [17]

$$G_{2M} = (S^2/2\pi) [G_{2M}^{(0)} / (1 + JG_{2M}^{(0)})], \quad (5)$$

where $G_{2M}^{(0)} = (2/N) \sum_q A_q^2 [\hbar\omega - 2\hbar\Omega_q]^{-1}$ is the noninteracting $2M$ Green function given in [17]. Here, A_q is a geometric factor, N is the number of cells, and Ω_q is the frequency of the magnon of wave vector \mathbf{q} (the wave vector of the pair is $\mathbf{k} = 0$).

The experiments were performed on single crystals of FeBO_3 at $T = 95$ K. Samples of dimensions $100 \times 100 \times 40 \mu\text{m}^3$ (larger surfaces cut normal to [111]) were cryogenically loaded into a Mao-Bell diamond-anvil cell [18] with the gasket filled with liquid argon; data using methanol ethanol (4:1) as the pressure-transmitting medium revealed no appreciable differences. After loading, the cell was mounted in the high-vacuum chamber of a specially designed optical cryostat operating in the range 85–300 K. The design allows one to change pressure from outside using a mechanical feedthrough. Temperature was controlled by varying the flow of liquid nitrogen through a copper block in thermal contact with the cell; the cryostat's drift is ~ 2 K on a 60-min time scale. For pressure calibration, we used the standard ruby fluorescence method [19]. The measured width of the ruby R lines at $P = 20$ GPa translates into $\Delta P \approx \pm 1$ GPa; this represents an upper limit for the dominant uncertainty due to nonhydrostatic contributions. Raman spectra, with $\sim 2 \text{ cm}^{-1}$ resolution, were obtained using a DILOR-XY multichannel system and 100 mW of 5145 Å focused to a spot of radius $\sim 20 \mu\text{m}$. Consistent with the low absorption of FeBO_3 below $\sim 4500 \text{ Å}$ [2], effects due to laser heating (as probed by, e.g., the width of the $2M$ band) were negligible. Unless stated otherwise, the polarizations of the incident and scattered light are perpendicular to [111], i.e., H_R is given by Eq. (4).

At ambient pressure, the energy of the E_g mode, $\hbar\omega_P$, lies above the cutoff of the $2M$ continuum at $\sim 4JSz$ [$z = 6$ is the number of nearest neighbors). With increas-

ing P , the magnetic scattering shifts rapidly enough so that it eventually resonates with and then overcomes the phonon. This is shown in Fig. 2. Compared with the internal mode, the $2M$ Grüneisen parameter is a factor of ~ 5.6 larger. Its actual value, $0.0178 \pm 0.0005 \text{ GPa}^{-1}$, is consistent with low-pressure measurements of T_N (at $P < 0.3 \text{ GPa}$) giving $\partial \ln T_N / \partial P = 0.0152 \pm 0.0008 \text{ GPa}^{-1}$ [20].

$$V = \frac{gS}{N^{1/2}} (\alpha + \alpha^\dagger) \sum_q A_q \{ (1 + 2 \sinh^2 \theta_q) (c_q c_{-q} + c_q^\dagger c_{-q}^\dagger) + \sinh \theta_q \cosh \theta_q (c_q^\dagger c_q + c_{-q}^\dagger c_{-q}) \}, \quad (6)$$

where g is the coupling constant, c_q and c_q^\dagger (α and α^\dagger) are magnon (phonon) operators, $\tanh(2\theta_q) = 1 - (\hbar \Omega_q / 2JSz)^2$ and $A_q = \cos(\mathbf{q} \cdot \mathbf{t}_1) - 2 \cos(\mathbf{q} \cdot \mathbf{t}_2) + \cos(\mathbf{q} \cdot \mathbf{t}_3)$. To order g^2 and approximating θ_q by zero (its value at the cutoff), the resulting width is $\Gamma_P \approx 2\pi g^2 S^2 \langle A_q^2 \rangle n_{2M} \times (\hbar \omega_P)$ with $\langle A_q^2 \rangle \approx \frac{9}{2}$. Here, the density of states n_{2M} is *not* the bare $2M$ density which diverges at the cutoff due to a van Hove singularity. Because V and the scattering term H_R [Eq. (4)] have the same form, one expects n_{2M} , like $G(\omega)$, to be strongly modified by magnon-magnon interactions; see Eq. (5). In $2M$ scattering, this coupling affects primarily the near-cutoff region by converting the divergency into a peak of width

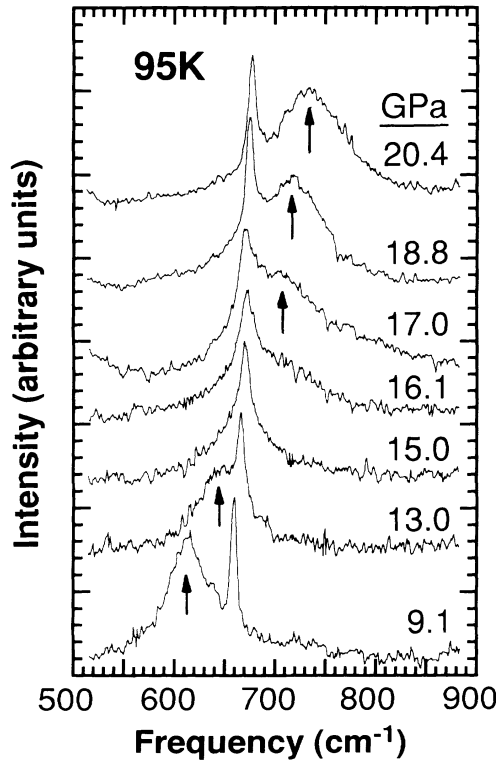


FIG. 2. Raman spectra at several pressures. The incident and scattered polarizations are normal to [111]. Arrows label the spin-pair continuum. The narrower feature at $660\text{--}680 \text{ cm}^{-1}$ is the $(\text{BO}_3)^{3-}$ in-plane bending mode.

The important features of our results reflecting the resonant interaction are the enhanced phonon width and the correlated intensity exchange in the range $P = 15\text{--}17 \text{ GPa}$ (Fig. 2). The measured *largest* additional full width at half maximum is $\Gamma_P = 10 \pm 3 \text{ cm}^{-1}$. Underlying the mode's shorter lifetime is its coupling to the large density of $2M$ states near the cutoff [17]. In terms of magnon variables and for the phonon component of Fig. 1, Eq. (3) becomes to lowest order (harmonic approximation)

$\approx 0.4(JSz)$ [14]. Assuming that these results apply to n_{2M} as well (see below), we infer from the experimental width $g = (0.16 \pm 0.02)J$.

The intensity behavior in the crossover region is well accounted for by Szigeti's coupled-mode theory with line shape given by [21]

$$I(\omega) = -\text{Im} \left\{ \frac{r_{2M}^2 G_{2M} - 2\Delta r_{2M} r_P G_{2M} G_P + r_P^2 G_P}{1 - \Delta^2 G_{2M} G_P} \right\}. \quad (7)$$

Here, $G_P = [\hbar \omega - \hbar \omega_P + i\gamma_P/2]^{-1}$, G_{2M} is the Green function of Eq. (5), and Δ is a phenomenological coupling constant. The normalization of G_{2M} gives $\Delta^2 \approx g^2 S^2 / 2$. Parenthetically, we note that $I(\omega)$ at $\gamma_P = 0$ is identical to the well-known expression derived by Fano applying to discrete-continuum interference [22]. Most of the parameters of Eq. (7) can be determined directly from the experiments (particularly from data where the peaks are well separated) and depend weakly on pressure. Not unexpectedly, the P dependence of J is the largest. As shown in Fig. 3, qualitative agreement with experiments performed in a wide pressure range can be achieved by varying J alone. We notice that the simulations accurately reproduce the intensity exchange and the larger width of the phonon in the resonant region. The agreement improves considerably by allowing the fixed parameters to be varied slightly and by including broadening effects due to pressure gradients. Specific examples emphasizing the dependence of the line shape on the configuration are shown in the inset of Fig. 3.

Consistent with the earlier estimate from Γ_P , the line-shape fits using Eq. (7) give $g = (0.20 \pm 0.07)J$. The relatively large value of g reflects the pronounced sensitivity of superexchange to variations of structural parameters [9]. A crude estimate of the coupling constant can be made by assuming that $J \propto l^\epsilon$ where l is, say, the Fe-O-Fe bonding length [9]. Thus, $g/J \sim \hat{Q} (\partial \ln J / \partial l) \sim \epsilon \hat{Q} / l$ with the phonon zero-point motion $\hat{Q} = \hbar / (2M \hbar \omega_P)^{1/2} \approx 0.04 \text{ \AA}$; note that $M \sim M_O \sim M_B$. For $g/J \sim 0.1$, one obtains the exponent $\epsilon \sim 10$. This value is of the same order of magnitude as those found in other Heisenberg anti-ferromagnets [9].

This work was supported in part by the U.S. Army

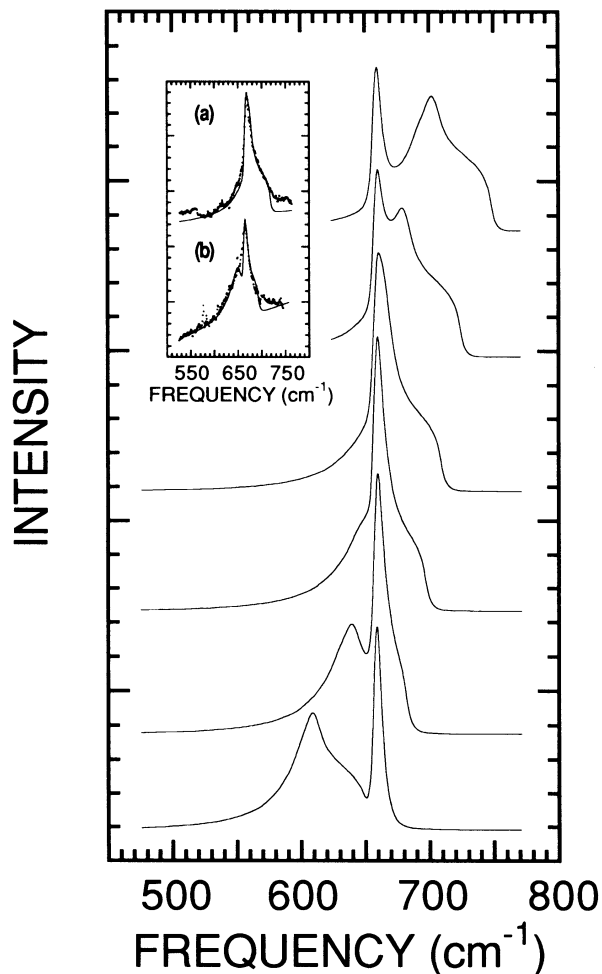


FIG. 3. Calculated spectra [Eq. (7)] simulating the data of Fig. 2. Line shapes have been convoluted with the instrument response function. From top to bottom, the traces correspond to J [cm^{-1}] = 12.5 (20.4), 12.15 (18.8), 12.0 (17.0), 11.66 (15.0), 11.3 (13.0), and 10.75 (9.0); values in parentheses are those of P [GPa] in Fig. 2. Other (fixed) parameters are $\Delta = 3 \text{ cm}^{-1}$, $r_{2M}/r_P = -2.0$, $\omega_P = 660 \text{ cm}^{-1}$, and $\gamma_P = 4 \text{ cm}^{-1}$. Note that, since only J is allowed to vary, the simulation values differ slightly from experimental ones inferred from the shift of the $2M$ peak. Inset: The dependence of the line shape on the scattering geometry (i.e., on the ratio r_M/r_P). Solid curves are fits to measurements at nearly the same pressure (≈ 16.5 GPa). Parameters are $\omega_P = 665.6 \text{ cm}^{-1}$, $J = 12.0 \text{ cm}^{-1}$ (a), 11.6 cm^{-1} (b) and $r_{2M}/r_P = -2.0$ (a), -2.5 (b). Spectrum (b) contains [111] polarized contributions.

Research Office (Contract No. DAAL-03-92-G-0233) and NSF DMR-9113911.

(a) Present address: Department of Physics, University of

Puerto Rico, University Station, San Juan, Puerto Rico 00931-3343.

- [1] C. M. Canali and S. M. Girvin, *Phys. Rev. B* **45**, 7127 (1992).
- [2] R. Wolfe, A. J. Kurtzig, and R. C. LeCraw, *J. Appl. Phys.* **41**, 1218 (1970).
- [3] W. Jantz, J. R. Sandercock, and W. Wettleing, *J. Phys. C* **9**, 2229 (1976).
- [4] D. C. Mattis, *The Theory of Magnetism I, Statistics and Dynamics*, Springer Series in Solid State Science Vol. 17 (Springer, Berlin, 1981).
- [5] J. M. Ziman, *Principles of the Theory of Solids* (Cambridge Univ. Press, Cambridge, 1979), p. 209.
- [6] Note that the leading term in Eq. (1) cannot couple phonons to one-magnon states (the process is forbidden by time-reversal symmetry). This is unlike systems for which the magnetic excitations have an orbital part where the dominant magnon-phonon coupling stems from spin-orbit interaction and phonon modulation of the crystal field; see J. B. Torrance and J. C. Slonczewski, *Phys. Rev. B* **5**, 4648 (1972).
- [7] L. C. Bartel and B. Morosin, *Phys. Rev. B* **3**, 1039 (1971), and references therein.
- [8] D. S. Fisher *et al.*, *Phys. Rev. Lett.* **61**, 482 (1988).
- [9] See, e.g., M. J. Massey *et al.*, *Phys. Rev. B* **42**, 8776 (1990).
- [10] J. W. Halley, *Phys. Rev.* **149**, 423 (1966); J. B. Sokoloff, *J. Phys. C* **5**, 2482 (1972).
- [11] Raman experiments on VI_2 providing indirect evidence of J modulation by zone-boundary phonons were reported by G. Güntherodt, W. Bauhofer, and G. Benedek, *Phys. Rev. Lett.* **43**, 1427 (1979).
- [12] N. Koshizuka *et al.*, *J. Phys. Soc. Jpn.* **37**, 354 (1974), and references therein.
- [13] See, e.g., M. Cardona, in *Light Scattering in Solids II*, Topics in Applied Physics Vol. 50, edited by M. Cardona and G. Güntherodt (Springer, Berlin, 1982), p. 45.
- [14] For reviews, see W. Hayes and R. Loudon, *Scattering of Light by Crystals* (Wiley-Interscience, New York, 1978), Chap. 7; M. G. Cottam and D. L. Lockwood, *Light Scattering in Magnetic Solids* (Wiley, New York, 1986).
- [15] M. J. Massey, Ph.D. thesis, The University of Michigan, 1992.
- [16] See K. Nakamoto, *Infrared Spectra of Inorganic and Coordination Compounds* (Wiley, New York, 1970), p. 90.
- [17] U. Balucani and V. Tognetti, *Phys. Rev. B* **8**, 4247 (1973).
- [18] H. K. Mao, P. M. Bell, K. J. Dunn, R. M. Chrenko, and R. C. Devries, *Rev. Sci. Instrum.* **50**, 1002 (1979), and references therein.
- [19] See, e.g., A. Jayaraman, *Rev. Mod. Phys.* **55**, 65 (1983).
- [20] D. M. Wilson, in *Magnetism and Magnetic Materials — 1976*, edited by J. J. Becker and G. H. Lander, AIP Conf. Proc. No. 34 (AIP, New York, 1976), p. 217.
- [21] B. Szigeti, *Proc. R. Soc. London A* **258**, 377 (1960).
- [22] U. Fano, *Phys. Rev.* **124**, 1866 (1961); see also D. Guidotti *et al.*, *Phys. Rev. Lett.* **43**, 1950 (1979), and references therein.

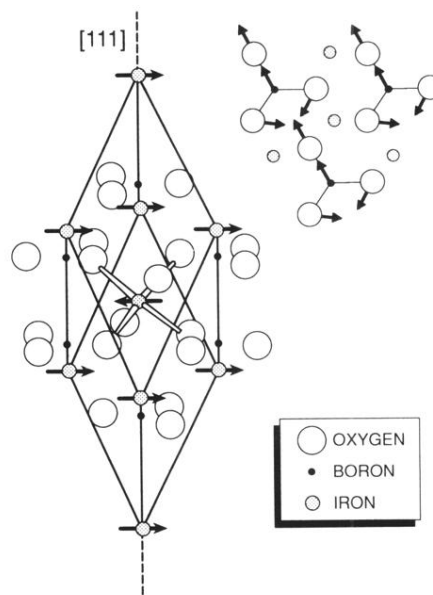


FIG. 1. Crystal structure of FeBO₃. The antiferromagnetic spin configuration is denoted by arrows attached to the cations. Inset: Three-layer projection on a (111) plane. The central Fe³⁺ ion and three (of a total of six) nearest cations and anions are indicated. Thinner arrows represent schematically one of the states of the doubly degenerate internal (BO₃)³⁻ mode.